

Chemical tagging of tidal tail star candidates of NGC 6362

Andrés E. Piatti¹

¹ Instituto Interdisciplinario de Ciencias Básicas (ICB), CONICET-UNCuyo, Padre J. Contreras 1300, M5502JMA, Mendoza, Argentina; andres.piatti@fcen.uncu.edu.ar

² Consejo Nacional de Investigaciones Científicas y Técnicas (CONICET), Godoy Cruz 2290, C1425FQB, Buenos Aires, Argentina

Received 20XX Month Day; accepted 20XX Month Day

Abstract The inner Milky Way disk globular cluster NGC 6362 appears to exhibit tidal tails composed of stars that have proper motions and positions in the color-magnitude diagram similar to those of cluster stars. Because recent results seem also to show that these stars are distributed across the regions least affected by interstellar absorption and reproduce the observed composite star field density map, we carried out a detailed spectroscopic analysis of a number of chemical element abundances of tidal tail star candidates in order to investigate the relationship of them with NGC 6362. From European Southern Observatory’s VLT@FLAMES spectra we found that the red giant branch stars selected as cluster’s tidal tail stars do not have overall metallicities nor abundances of Mg, Ca, Sc, Ti, Cr, Ni and Ba similar to the cluster’s ones. Moreover, they are mainly alike to stars that belong to the Milky Way thick disk, some of them could be part of the thin disk and a minor percentage could belong to the Milky Way halo star population. On the other hand, since the resulting radial velocities do not exhibit a distribution function similar to that of cluster’s stars, we concluded that looking for kinematic properties similar to those of the cluster would not seem to be an approach for selecting cluster’s tidal tail stars as suitable as previously thought.

Key words: globular clusters:general – globular clusters:individual:NGC 6362 – methods: observational – techniques:spectroscopic

1 INTRODUCTION

Recently, Zhang et al. (2022) published a stringent compilation of Milky Way globular clusters with robust detection of extra-tidal structures. Their catalog includes 46 globular clusters classified as follows: 27 with tidal tails, 4 with extended envelopes, and 15 without observed extended features. The detection of tidal tails around Milky Way globular clusters is a research avenue of significant importance for our understanding of a wide variety of issues. For instance, globular clusters associated to destroyed dwarf progenitors should show tidal tails (Carballo-Bello et al. 2014; Mackey et al. 2019); globular clusters formed in dark matter mini-halos should present tidal tails with a relatively large velocity dispersion (Malhan et al. 2021); the extension and shape of tidal tails tell us about the dynamical history of a globular cluster as a consequence of its interaction with the Milky Way (Hozumi & Burkert 2015; de Boer et al. 2019), etc.

The innermost globular cluster in the Zhang et al. (2022)’s compilation is NGC 6362 (galactocentric distance $R_{GC} = 5.5$ kpc; Baumgardt & Vasiliev 2021), which shows tidal tails. Zhang et al. (2022)

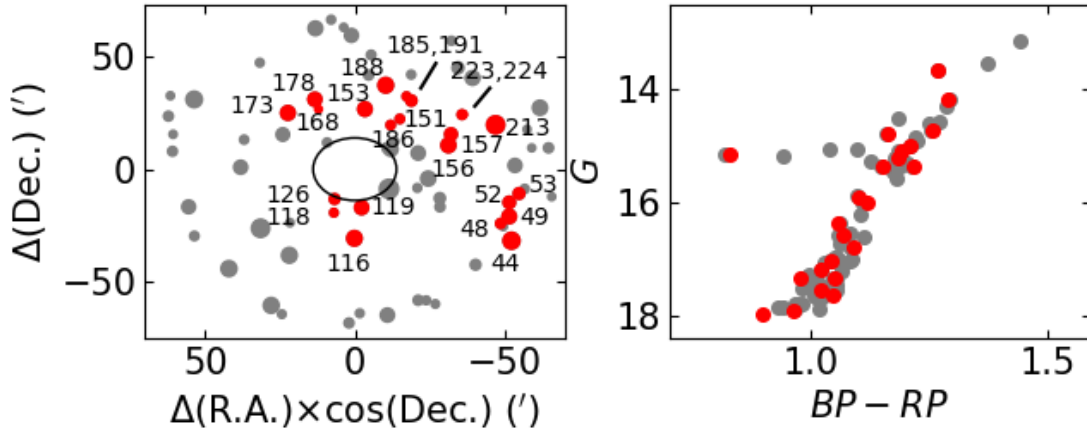


Fig. 1: Spatial distribution of Kundu et al. (2019)’s tidal tail stars (left panel), and their location in the color-magnitude diagram (right panel). Red symbols represent the stars observed in this work. In the left panel, the size of the symbol is proportional to the star’s brightness, and the black circle represents the cluster’s Jacobi radius (Moreno et al. 2014).

included NGC 6362 as a globular cluster with tidal tails based on the work of Kundu et al. (2019), who found 73 highest-ranked extra-tidal red giants with *Gaia* DR2 proper motions within 3-sigma around the mean cluster proper motion. However, escaping stars should show a dispersion velocity larger than that for outermost bound stars (Wan et al. 2021; Piatti 2023), which is not the case of these 73 extra-tidal giant candidates. On the other hand, NGC 6362 should not have tidal tails composed by kinematically cold stars, because Kundu et al. (2019) showed that the orbit of NGC 6362 is chaotic, which means that it washes out (accelerating) those stars (Mestre et al. 2020). What we mention above is a strong motivation for deciphering whether NGC 6362 already pertain to the group of globular clusters with observed tidal tails, making it a compelling science case because its position in the inner Milky Way. Precise abundances of some chemical elements for Kundu et al. (2019)’s highest-ranked extra-tidal stars could provide the final link between the extra tidal star candidates and NGC 6362. Indeed, we assumed that chemical abundances significantly deviating from the mean values known for NGC 6362 point to a star formation scenario not related to that of the cluster itself.

Precisely, we embarked in an observational campaign with the aim of obtaining spectra of these selected stars with the aim of deriving abundances of different chemical elements and hence to investigate their relationship with NGC 6362. Likewise, the results will be helpful to assess on the validity of some criteria used to select these stars as highest-ranked extra-tidal stars. In other words, we attempt to shed light about the suitability of the frequently applied criterion to detect tidal tails based on similar proper motions for cluster members and tidal tail stars (e.g., Sollima 2020). In Section 2 we present the acquired observational material, and in Section 3 we derive different astrophysical properties of the target stars. Section 4 is devoted to the discussion on their chemical element abundances. Finally, Section 5 summarizes the main conclusions of this work.

2 OBSERVATIONAL DATA

The red giant stars selected by Kundu et al. (2019) as tidal tail candidates of NGC 6362 have proper motions within 3σ of the mean cluster proper motion (Vasiliev 2019). They are also located beyond the cluster Jacobi radius (Moreno et al. 2014), and are distributed in the color-magnitude diagram along the cluster red giant branch. Figure 1 illustrates their spacial distribution and their location in the cluster color-magnitude diagram (figure built from Table 3 of Kundu et al. 2019). We accommodated as many stars as possible across the FLAMES spectrograph’s field-of-view (Pasquini et al. 2002) attached at the European Southern Observatory (ESO)’s Very Large Telescope (programme 113.2661.001, PI:Piatti).

By applying the completeness expression of Piatti (2017), which allowed us to take into account the tidal tail stars' spatial coverage and their distribution in the color-magnitude diagram, we found that the finally selected star sample, represented with red circles in Figure 1, statistically represents $\sim 80\%$ of the whole Kundu et al. (2019)'s red giant sample brighter than $G = 18.0$ mag.

We used the FLAMES@GIRAFFE spectrograph with the MEDUSA 132 fiber component and the HR14 grism ($\sim 6290\text{--}6690$ Å), which gives a dispersion of 0.05 Å/pixel with a resolution of $R = 17000$, appropriate to measure abundances of different chemical elements with an accuracy enough to chemically distinguish stars formed in NGC 6362 or elsewhere. We obtained spectra of the selected stars from a total exposure time of 2235 sec per observed science field (five different pointings), and typical airmass and seeing of $\sim 1.34\text{--}1.45$ and $0.45''\text{--}0.76''$, respectively. Fifteen sky spectra were also taken simultaneously to each science field.

The data were processed in the standard way, following the FLAMES@GIRAFFE ESO pipeline¹, which includes zero-subtraction, flat-field correction, wavelength calibration with a standard Th-Ar lamp, extraction of one-dimensional spectra, etc. By comparing the observed position of several sky emission lines with their rest-frame position using the sky lines atlas by Osterbrock et al. (1996), we checked that there does not exist any significant wavelength shifts. Finally, the sky-subtracted spectra were extracted from all the multi-object spectroscopy exposures. Table 1 lists the observed stars alongside with their equatorial coordinates, *Gaia* DR3 (Gaia Collaboration et al. 2016; Babusiaux et al. 2022) photometry, and average signal-to-noise ratio (S/N) along the whole wavelength range of each spectrum. One science field, which includes stars #116, 118, 119 and 126 was observed in two different night, the first one under no good weather conditions. From this night, only the spectrum of #116 could be extracted with a reasonable S/N ratio. Therefore, we used the spectra of star #116 coming from both nights to check internal consistency in the radial velocity and chemical element abundance measurements.

Finally, we retrieved from the ESO archive² the processed spectra of NGC 6362's red giants taken with FLAMES@GIRAFFE and an instrument setup similar to ours (programme 093.D-0618(A), PI: Dalessandro). The main aim of dealing with this data is to validate our procedure of deriving abundances of chemical elements, by comparing the present resulting values with those of Mucciarelli et al. (2016)

3 STELLAR PARAMETERS AND ABUNDANCE ANALYSIS

3.1 Radial velocity measurements

We measured radial velocities (RVs) by cross-correlating the observed spectra and the Arcturus spectrum taken from Hinkle et al. (2000)³. All the spectra were continuum normalized before the cross-correlation procedure and the Arcturus spectrum spectral resolution was degraded to match the resolution of our science spectra. We made use of the IRAFFXCOR task, which implements the algorithm described in Tonry & Davis (1979) for the construction of the cross-correlation function of each (object, Arcturus) spectra pair. In addition to the RVs, FXCOR returns the CCF normalized peak (h), which is an indicator of the degree of similarity between the correlated spectra and the Tonry & Davis ratio (TDR) defined as $TDR = h/(\sqrt{2}\sigma_a)$, where σ_a is root mean square of the CCF antisymmetric component. The resulting RVs are associated to h values greater than 0.8. We finally carried out the respective heliocentric corrections by using the IRAF task RVCORRECT. Table 1 lists the resulting heliocentric RVs with their respective uncertainties. The difference in the RVs measured for star #116, observed in two different nights, resulted to be 0.00 ± 0.41 km/s, where the error comes from the propagation of both individual RV uncertainties. We compared our resulting RVs with those of *Gaia* DR3 for four stars in common (# 44, 116, 188 and 213)) and found a difference (*Gaia* DR3 - our) of 0.14 ± 1.28 km/s.

¹ <http://www.eso.org/sci/software/pipelines/>

² https://archive.eso.org/eso/eso_archive_main.html

³ https://www.eso.org/sci/observing/tools/uvespop/bright_stars_uptonow.html

Table 1: Astrophysical properties of studied stars.

ID	R.A. ($^{\circ}$)	Dec. ($^{\circ}$)	G (mag)	BP (mag)	RP (mag)	$\langle S/N \rangle$	RV (km/s)	T_{eff} (K)	$\log g$	v_t (km/s)	[Fe/H] (dex)
44	260.696624999996	-67.57813888888806	14.16	14.72	13.45	65.8	-24.67 \pm 0.37	4800	2.80	1.30	0.00 \pm 0.05
48	260.865999999996	-67.45077777777699	17.03	17.46	16.44	19.2	-22.93 \pm 0.46	5250	3.20	2.00	0.00 \pm 0.08
49	260.746333333329	-67.39899999999916	15.20	15.70	14.53	34.1	-100.03 \pm 1.18	4800	1.50	1.55	-1.37 \pm 0.08
52	260.755333333329	-67.29455555555468	16.00	16.46	15.36	30.7	208.71 \pm 0.84	5050	2.60	4.00	-1.13 \pm 0.06
53	260.621541666662	-67.22872222222135	16.36	16.79	15.75	24.4	-22.03 \pm 1.15	5250	3.00	2.65	-1.30 \pm 0.15
116	262.984874999996	-67.56041666666580	14.78	15.26	14.12	56.3	-92.06 \pm 0.41	4870	2.80	1.50	-0.43 \pm 0.06
118	263.281416666662	-67.37069444444360	17.63	18.07	17.04	19.4	-8.83 \pm 0.73	5180	3.80	1.50	-0.42 \pm 0.09
119	262.881083333329	-67.33286111111025	15.33	15.85	14.60	43.3	-13.82 \pm 0.76	4880	2.40	1.00	-0.66 \pm 0.09
126	263.269999999996	-67.2690833333249	16.76	17.22	16.15	25.2	-13.75 \pm 0.99	5100	3.40	2.00	-0.70 \pm 0.10
151	262.474458333329	-66.72133333333246	17.33	17.73	16.77	23.8	50.12 \pm 1.34	5300	1.80	1.50	0.02 \pm 0.13
153	262.346874999996	-66.67613888888799	17.33	17.76	16.72	23.9	-3.34 \pm 0.83	5080	3.50	1.20	-0.81 \pm 0.06
156	261.654583333329	-66.87124999999916	14.99	15.50	14.31	67.0	46.16 \pm 0.48	4860	2.40	1.50	-0.33 \pm 0.07
157	261.622874999996	-66.78972222222137	15.88	16.32	15.23	43.7	-111.37 \pm 0.64	5170	3.10	1.00	-0.20 \pm 0.09
168	263.486999999996	-66.60394444444357	17.96	18.30	17.43	16.5	-70.81 \pm 1.00	5550	3.30	4.00	-0.55 \pm 0.05
173	263.916249999996	-66.63174999999915	15.06	15.56	14.39	67.2	-81.34 \pm 0.57	4930	2.50	1.20	-0.67 \pm 0.05
178	263.536291666662	-66.53094444444356	15.33	15.81	14.68	39.3	39.50 \pm 0.44	4900	2.60	1.20	-0.90 \pm 0.06
185	262.252874999996	-66.50902777777696	17.53	17.96	16.96	23.0	-106.39 \pm 1.34	5230	3.60	5.00	-0.86 \pm 0.08
186	262.837666666662	-66.60333333333248	15.15	15.46	14.65	50.8	34.48 \pm 0.50	5710	3.10	5.00	-1.00 \pm 0.15
188	262.549666666662	-66.42669444444357	14.71	15.25	14.01	65.2	15.91 \pm 0.39	4850	2.20	1.25	-0.20 \pm 0.07
191	262.189499999996	-66.54047222222139	16.56	17.00	15.95	33.4	34.45 \pm 0.63	5140	3.15	5.00	-0.49 \pm 0.12
213	260.999708333329	-66.71997222222140	13.65	14.20	12.95	88.3	-71.84 \pm 0.30	4820	2.50	1.40	-0.16 \pm 0.08
223	261.477583333329	-66.64430555555467	17.17	17.59	16.59	22.8	56.95 \pm 0.87	5330	3.80	2.40	-0.05 \pm 0.06
224	261.457291666662	-66.64280555555466	17.90	18.29	17.35	18.6	-27.65 \pm 0.73	5360	3.60	5.00	-0.60 \pm 0.10

3.2 Stellar atmospheric parameters

With the aim of obtaining initial estimates of effective temperature (T_{eff}) and surface gravity ($\log g$) for chemical abundance analysis, we derived photometric parameters using the *Gaia* DR3 photometry (see Table 1). The effective temperatures were computed from *Gaia* $BP - RP$ colors, previously corrected by interstellar absorption using the $E(B - V)$ values of Piatti (2024) and the total to selective absorption ratios given by Chen et al. (2019). The reddening corrected $(BP - RP)_o$ colors were then transformed to Johnson $(R - I)_o$ ones using the transformation equations derived by Pancino et al. (2022). Finally, we employed the suitable correlation between the free metallicity sensitivity Johnson $(R - I)_o$ color and T_{eff} derived by Alonso et al. (1999). The surface gravity was calculated using the equation $\log g = 4.44 + \log M_* + 4 \log T_{eff}/5780 + 0.4(V_o - (m - M)_o) + BC(V) - 4.75$ (Venn et al. 2017), where $M_* = 0.75$ is the typical mass of an old red giant branch star; V_o is the dereddened Johnson V magnitude (calculated from (Pancino et al. 2022)’s transformation equations); $(m - M)_o = 14.42$ mag (Baumgardt & Vasiliev 2021) is the true cluster distance modulus; and $BC(V)$ is the Alonso et al. (1999, eq. 18) bolometric correction, for which we adopted a cluster mean metallicity $[Fe/H] = -1.07 \pm 0.01$ dex (Massari et al. 2017).

We derived spectroscopic T_{eff} , $\log g$ and microturbulent velocity of the studied stars together with $[Fe/H]$ values based on excitation and ionization equilibrium. The equivalent widths (EWs) of Fe I and Fe II lines and those of other species (Mg, Ca, Sc, Ti, Cr, Ni, Ba) were measured using DAOSPEC (Stetson & Pancino 2008) and its up-to-date internal list of more than 400 lines, with their respective oscillator strengths and excitation potentials. We alternatively checked the EW values of weak lines by using the IRAF.SPLOT routine to manually measure the EWs. From the resulting EW list, we removed those lines with no EW value or with $q > 1$; q is a quality parameter derived from a comparison between the residuals observed in the spectrum in the immediate neighborhood of the line and the typical residuals in the spectrum as a whole.

The spectral line analysis to determine the chemical composition of the stars was performed with MOOG (Sneden 1973; Sobeck et al. 2011). MOOG asks mainly for two inputs, namely, a line data file and a model atmosphere file. The former is mainly the above resulting DAOSPEC output, with some

Table 2: Chemical abundances of the studied stars.

ID	[Mg/Fe] (dex)	[Ca/Fe] (dex)	[Sc/Fe] (dex)	[Ti/Fe] (dex)	[Cr/Fe] (dex)	[Ni/Fe] (dex)	[Ba/Fe] (dex)
44	—	0.08±0.10	-0.12±0.12	0.07±0.07	—	0.04±0.12	—
48	—	-0.03±0.09	—	0.05±0.12	0.01±0.10	-0.03±0.13	—
49	—	0.20±0.09	—	—	—	0.05±0.13	0.03±0.15
52	0.31±0.12	0.17±0.12	—	—	—	0.08±0.12	—
53	—	—	—	—	—	—	—
116	0.37±0.15	0.02±0.14	0.19±0.15	0.20±0.10	0.00±0.15	0.04±0.15	—
118	0.44±0.10	-0.11±0.13	0.08±0.14	0.16±0.14	—	-0.02±0.14	-0.15±0.16
119	—	0.05±0.12	—	0.16±0.13	—	-0.03±0.12	-0.08±0.16
126	—	0.20±0.14	—	0.25±0.15	—	0.03±0.14	—
151	—	0.03±0.17	—	0.02±0.18	—	-0.09±0.19	—
153	0.41±0.12	0.32±0.11	—	0.06±0.15	—	0.00±0.12	-0.03±0.15
156	—	0.13±0.10	0.13±0.13	0.18±0.13	0.08±0.12	0.02±0.13	—
157	0.27±0.10	0.00±0.12	0.12±0.14	0.05±0.14	0.09±0.14	0.08±0.12	0.06±0.16
168	0.39±0.12	0.17±0.12	—	0.20±0.12	0.05±0.12	0.05±0.12	-0.09±0.14
173	—	0.05±0.10	-0.02±0.08	—	—	0.01±0.08	-0.04±0.14
178	—	0.09±0.09	—	0.05±0.12	—	0.18±0.06	0.02±0.15
185	—	0.24±0.14	—	0.32±0.14	—	—	—
186	—	—	—	—	—	—	—
188	0.24±0.08	0.10±0.11	-0.05±0.11	0.00±0.11	-0.11±0.12	0.06±0.12	—
191	—	0.15±0.16	—	0.17±0.17	—	0.10±0.16	—
213	0.16±0.13	0.01±0.12	0.13±0.13	0.11±0.11	-0.09±0.13	-0.03±0.11	—
223	—	0.16±0.12	0.12±0.12	0.03±0.12	0.09±0.12	0.03±0.11	—
224	0.30±0.11	0.20±0.14	0.10±0.15	0.15±0.15	0.05±0.13	0.06±0.15	-0.10±0.17

slight different format arrangement. For the latter, we adopted the Kurucz (2005)'s models generated with the ATLAS code (Kurucz 1970). The models were interpolated for any set of (T_{eff} , $\log g$, v_t , [Fe/H]) using the Python interpolator `PyKMOD`⁴. We started by interpolating the models with the photometric T_{eff} and $\log g$ values, and then by running MOOG to obtain chemical element abundances. We iterated this loop until reaching convergence at $\Delta T_{eff} = 5\text{K}$, $\Delta \log g = 0.05$ and $\Delta v_t = 0.05\text{ km/s}$. In order to reach excitation and ionization equilibrium, the program simultaneously: 1) varies the values of T_{eff} looking for a zero slope in the (FeI, FeII) abundance versus excitation potential relationship; 2) varies v_t looking for a zero slope in the FeI abundance versus wavelength relationship; and 3) varies $\log g$ looking for similar FeI and FeII abundance values. Since FeI and FeII abundance values changed as well, each iteration is fed by an interpolated model with the updated overall metallicity. During the chemical abundance analysis we removed some chemical elements with only one EW measure. The resulting stellar atmospheric parameters (T_{eff} , $\log g$, v_t and [Fe/H]) are listed in Table 1. The mean and dispersion of [Fe/H] come from the average of all FeI and FeII abundance values. Table 2 lists the mean and dispersion of the remaining measured chemical elements, corresponding to the final adopted stellar atmosphere model. They correspond to the standard deviation of all the available chemical element abundance values, which in turn come from the final atmospheric parameters adopted according to the convergence uncertainties mentioned above. The difference between the abundance values obtained for star #116 observed in two different nights resulted to be 0.00-0.07 dex, depending on the chemical element. As for the NGC 6362's red giants we obtained a mean metallicity of [Fe/H] = -1.08 ± 0.03 dex, in excellent agreement with Mucciarelli et al. (2016), so that we did not apply correction to our metallicities due to systemic errors.

⁴ <https://github.com/kolecki4/PyKMOD>

4 ANALYSIS AND DISCUSSION

NGC 6362 has been recently targeted with the aim of accurately estimating its astrophysical properties. Massari et al. (2017) obtained ESO@FLAMES.UVES high-resolution spectra for 11 cluster red giant branch stars and derived a mean cluster RV and $[\text{Fe}/\text{H}]$ of -15.03 ± 2.07 km/s and -1.07 ± 0.01 dex, respectively. They also derived mean cluster abundances of 17 chemical elements, among them $[\text{Mg}/\text{Fe}] = 0.54 \pm 0.01$ dex, $[\text{Ca}/\text{Fe}] = 0.26 \pm 0.02$ dex, $[\text{Sc}/\text{Fe}] = 0.18 \pm 0.02$ dex, $[\text{Ti}/\text{Fe}] = 0.24 \pm 0.04$ dex, $[\text{Cr}/\text{Fe}] = -0.05 \pm 0.04$ dex, $[\text{Ni}/\text{Fe}] = -0.02 \pm 0.01$ dex, and $[\text{Ba}/\text{Fe}] = 0.61 \pm 0.01$ dex. We used this cluster chemical tagging to assess on the origin of a representative sample of stars selected by Kundu et al. (2019) as cluster's tidal tail candidates.

There are several relevant implications from the existence or not of NGC 6362's tidal tails, among them whether its tidal tails are kinematic cold or hot, whether NGC 6362 is in a regular or chaotic orbital motion; or at what extend criteria of detected globular clusters' tidal tails based on kinematic properties are appropriate. Some recent result focused on the analysis of deep images across an area of ~ 4 squared degree centered on the cluster (Piatti 2024), converged toward a relatively smooth stellar density between 1 and ~ 3.8 cluster Jacobi radii, with a slight difference smaller than two times the background stellar density fluctuation between the mean stellar density of the South-eastern hemisphere and that of the North-western one, with the latter being higher. Moreover, the spatial distribution of Kundu et al. (2019)'s tidal tail stars agrees well not only with the observed composite star field distribution, but also with the region least affected by interstellar absorption. These results would seem to suggest that NGC 6362 would not have clearly detectable tidal tails.

The identification of globular cluster's tidal tail stars has been frequently addressed by looking for stars that are kinematically consistent with the mean kinematic properties of globular clusters where the stars formed (Sollima 2020; Xu et al. 2024). However, rather than looking for kinematic properties (proper motions, RVs) similar to the cluster's ones, it has been suggested in the recent literature to focus on the dispersion of the radial and tangential velocities, as well as in the z-component of the angular momentum (Malhan et al. 2021, 2022). This approach would seem more suitable to describe the kinematic properties of tidal tail stars, since stars in order to escape from the cluster need to reach velocities different than those of cluster's members. Then, the Milky Way potential imprints on them different accelerations, so that mean kinematic properties vary along tidal tail extensions (Piatti et al. 2023; Grondin et al. 2024). In order to identify tidal tail stars following this approach, the knowledge of the mean path of cluster's tidal tail stars in the kinematic space is required, which according to Grillmair (2025, and references therein) can be obtained by combining color-magnitude diagram and kinematic filtering with orbit integration and predictions based on modeling the stripping stars. Alternatively, a kinematic analysis of the sample stars following the approach described in Nissen & Schuster (2010), including the use of a Toomre diagram, could also more clearly indicate whether they belong to the thin disk, thick disk, or halo populations. Since the main aim of this study is to assess on the formation scenario of Kundu et al. (2019)'s selected stars, we defer such an analysis for a future work.

In this context, we probed whether the RVs of Kundu et al. (2019)'s tidal tail stars are consistent with the mean cluster's RV, by comparing the resulting RVs (Table 1) with the mean RV value of NGC 6362. We found that two stars (#119 and 126) fall within 1σ , and other twelve stars (#44, 48, 49, 53, 116, 118, 157, 168, 173, 185, 223 and 224) are within 3σ , which represent $\sim 9\%$ and $\sim 60\%$ of the studied star sample, respectively. Figure 2 illustrates this finding. We recall that the stars selected by Kundu et al. (2019) are within 3σ of the mean cluster's proper motion. The above outcome suggests that even in the most relaxed scenario (RV statistics within 3σ), a significant percentage of the star sample are not coherent with the mean cluster's RV, as it is the case when proper motions are considered. This discrepancy calls our attention on the possible weakness of selection criteria of tidal tail stars based on their kinematic properties. Furthermore, if we restricted the range of RVs to 1σ of the mean cluster's RV, the small number of stars that comply with that requirement tells us that either the 3σ sample is contaminated by field stars (because of the large difference in the number of stars between 1σ and 3σ samples) or tidal tail stars reach kinematic properties different than those of the cluster soon after escaping it (because of the spread in RV of stars located just outside the Jacobi radius).

In order to find more conclusive evidence on the origin of the studied stars, i.e., to confirm or dismiss that the studied stars formed in NGC 6362, we analyzed their chemical properties (Hanke et al. 2020, and references therein). Unlike kinematic features, the abundance of chemical elements remains almost unchanged along the stellar lifetimes. To this respect, Marino et al. (2019) showed that the metallicity difference between first and second generation stars in NGC 6362 is $\Delta[\text{Fe}/\text{H}] = 0.03$ dex. We then compared the resulting $[\text{Fe}/\text{H}]$ values with the mean metallicity of NGC 6362 and found that the difference $[\text{Fe}/\text{H}]_{\text{star}} - [\text{Fe}/\text{H}]_{\text{NGC6362}}$ is smaller than the respective associated errors added in quadrature only for stars #52 and 186. Indeed, Figure 2 shows that the spread in metallicity of the studied stars is as large as the metallicity dispersion found in the Milky Way disk star field population (see below). On the other hand, star #52 has different Mg, Sc, Ti, Cr, and Ba abundances than NGC 6362’s red giants (see Massari et al. 2017), while star #186 does not share with NGC 6362 any of the estimated chemical element abundances. Furthermore, their RVs are remarkably different from that of the cluster (they are placed just outside the cluster’s Jacobi radius), even though we assumed that tidal tail star can have RVs different from the mean cluster’s RV. Therefore, it would seem to be unlikely that any of the studied stars have formed in NGC 6362.

The obtained chemical tagging results lead us to conclude that some Milky Way field stars located along the line-of-sight toward NGC 6362 can have proper motions and positions in the color-magnitude diagram consistent with the mean cluster’s proper motion and cluster’s sequences in the color-magnitude diagram (Kundu et al. 2019). However, although the latter would seem to be a valid selection criterion, the former would not. Indeed, kinematics of highest ranked tidal tail stars can show variation of their motions along the tidal tails, as judged by some observational (Piatti 2023; Grillmair 2025) and theoretical (Grondin et al. 2024) results, among others.

We finally took advantage of the abundances derived for some chemical elements in order to further constrain the origin of the studied stars. To this respect, we made use of different compilations of Milky Way thick and thin disk and halo field stars, namely: Reddy et al. (2003, thick disk); Venn et al. (2004, thick and thin disks and halo); Reddy et al. (2006, thick disk); and Nissen & Schuster (2010, halo), and built Figure 3. As can be seen, the $[\text{X}/\text{Fe}]$ trend with $[\text{Fe}/\text{H}]$ has a slope close to zero for Cr and Ni, so that no clear difference comes up for the three field star populations. In the case of Ba, we did not find any measures for halo stars available. From Mg, Ca and Ti relationships it is possible to distinguish a somehow bimodal distribution along the Y-axis for thick disk field stars with some overlap of thin disk field stars around the most metal-poor peak. Halo stars in general expand the whole measured range of these chemical element abundances, mainly populating much metal-poor overall metallicities. From this scenario, we speculate with the possibility that most of the studied stars belong to the Milky Way disk; some could be part of the thin disk, and a minor percentage might be halo stars.

5 CONCLUSIONS

We embarked in a spectroscopic tagging analysis of a sample of stars cataloged as tidal tail star candidates of the Milky Way globular cluster NGC 6362. The importance of confirming their status as cluster’s escaped stars relies on the consequences for our understanding of globular cluster formation and evolution, and hence for arriving to a general consensus about the applicable procedures in searching for globular cluster tidal tail stars. From measures of individual radial velocities, metallicities, and abundances of some chemical elements, we disentangled whether the studied stars formed in NGC 6362 and were later unbound from the cluster’s body due to the interaction with the Milky Way. We concluded that:

- Despite the similar values derived of some particular properties for some stars, none of the studied stars would seem to share the mean cluster chemical element abundances within the estimated uncertainties. Therefore, the selected stars, which statistically represent nearly 80% of all the red giant branch tidal tail candidates, would not seem to be formed in NGC 6362. From the lack of confirmation of red giant branch tidal tail stars, we speculate that NGC 6362 does not have detected tidal tails. This conclusion agrees with the recent outcome by Piatti (2024) who showed that the spatial distribution of

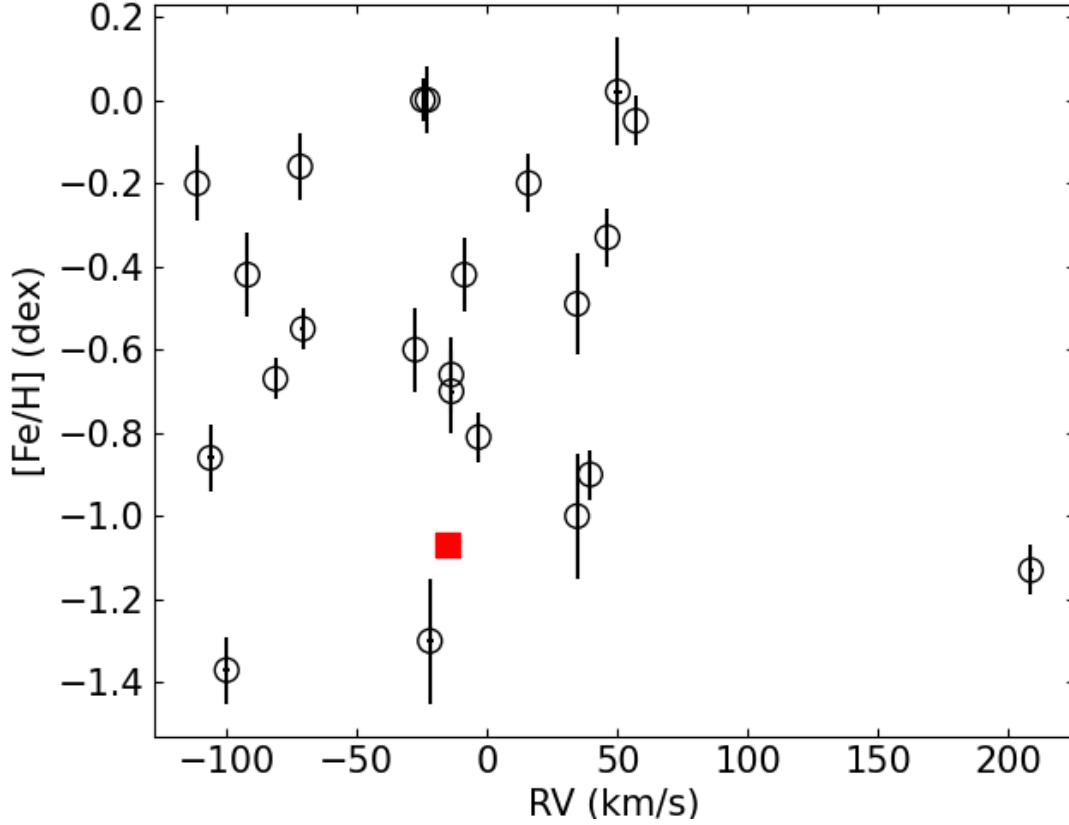


Fig. 2: $[\text{Fe}/\text{H}]$ vs RV relationship for the studied stars (open circles, Table 1) and for NGC 6362 (red box, Massari et al. 2017).

the tidal tail star candidates remarkably matches that of the observed composite star field distribution, and the regions least affected by interstellar absorption.

- In agreement with the above result, the measures of individual radial velocities cover a wide range of values, typical of stars belonging to the composite Milky Way field star population. Although variation in the radial velocities of tidal tail stars are expected -this is not the case, because they have different metallicities-, our present values contrast with their similar proper motions within 3σ , and with their location along the red giant branch in the cluster color-magnitude diagram (Kundu et al. 2019). This means that kinematics properties would not seem to be as suitable as previously thought for searching globular cluster tidal tails. Beyond the uncertainties in the *Gaia* DR2 data that could lead to incur in considering some field stars as cluster tidal tail candidates, the criterion of filtering stars with similar mean globular cluster kinematics would not seem appropriate. This is because tidal tails already exhibit a coherent variation of the star motions along them.

- The observed stars, distributed along the line-of-sight toward NGC 6362, would seem to belong mainly to the thick disk, as judged by the derived abundances of some chemical elements in comparison with previous compilations of Milky Way field stars. We do not discard the possibility that some of them pertain to the thin disk, an even a small percentage to the Milky Way halo. The outcome that the studied stars could be Milky Way field stars agrees well with the cluster having a chaotic orbit (Kundu et al. 2019), which means that its tidal tails were swept while approaching the innermost Milky Way regions.

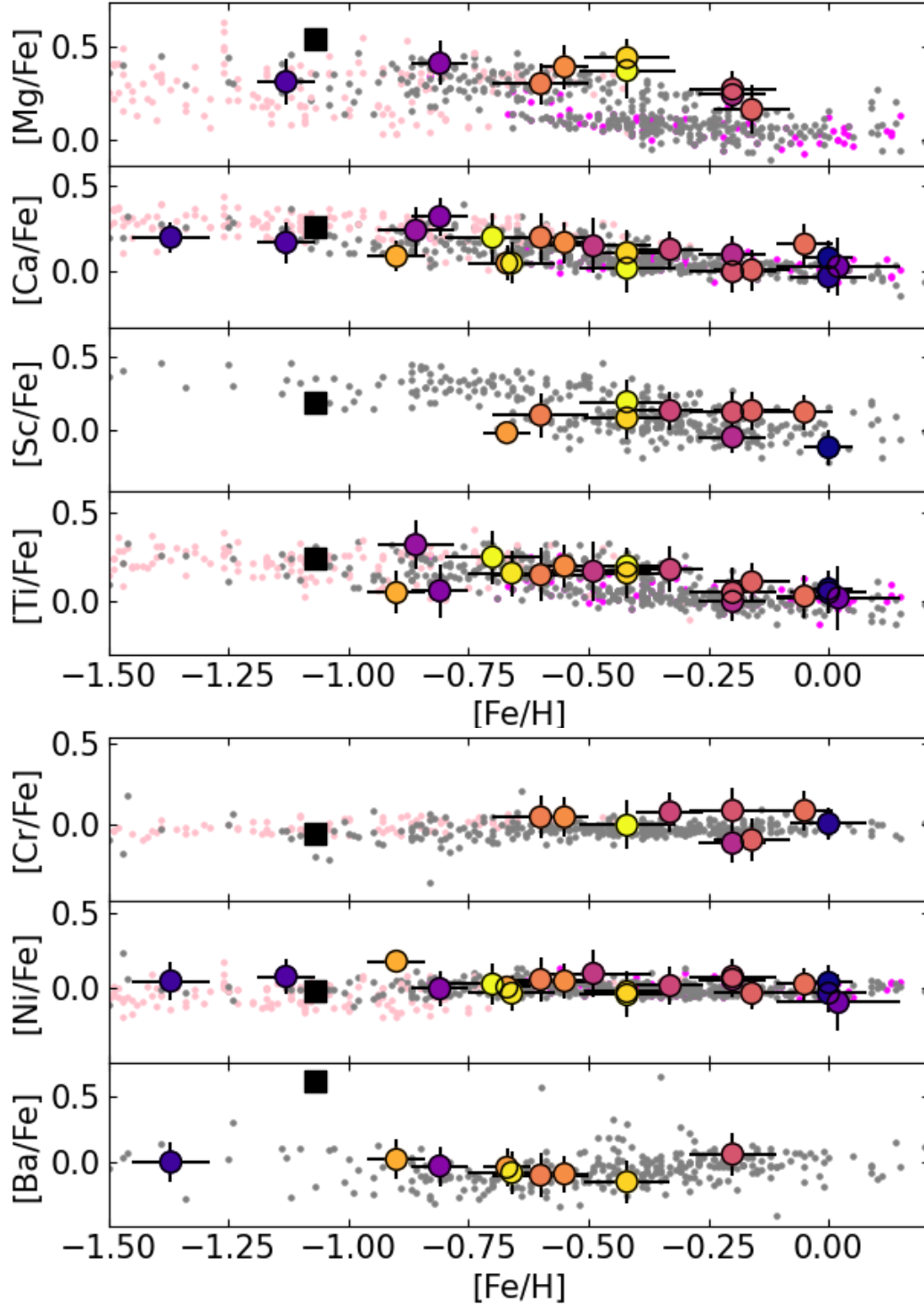


Fig. 3: $[X/Fe]$ vs $[Fe/H]$ relationships for the studied stars. Small magenta, gray and pink dots represent Milky Way thin and thick disks and halo field stars, respectively. The large black square represents NGC 6362.

Acknowledgements We thank the referee for the thorough reading of the manuscript and timely suggestions to improve it.

Based on observations collected at the European Southern Observatory under ESO programme(s) 113.2661.001.

Data for reproducing the figures and analysis in this work will be available upon request to the author.

References

- Alonso, A., Arribas, S., & Martínez-Roger, C. 1999, *A&AS*, 140, 261 4
- Babusiaux, C., Fabricius, C., Khanna, S., et al. 2022, arXiv e-prints, arXiv:2206.05989 3
- Baumgardt, H., & Vasiliev, E. 2021, *MNRAS*, 505, 5957 1, 4
- Carballo-Bello, J. A., Sollima, A., Martínez-Delgado, D., et al. 2014, *MNRAS*, 445, 2971 1
- Chen, B. Q., Huang, Y., Yuan, H. B., et al. 2019, *MNRAS*, 483, 4277 4
- de Boer, T. J. L., Gieles, M., Balbinot, E., et al. 2019, *MNRAS*, 485, 4906 1
- Gaia Collaboration, Prusti, T., de Bruijne, J. H. J., et al. 2016, *A&A*, 595, A1 3
- Grillmair, C. J. 2025, *ApJ*, 979, 75 6, 7
- Grondin, S. M., Webb, J. J., Lane, J. M. M., Speagle, J. S., & Leigh, N. W. C. 2024, *MNRAS*, 528, 5189 6, 7
- Hanke, M., Koch, A., Prudil, Z., Grebel, E. K., & Bastian, U. 2020, *A&A*, 637, A98 7
- Hinkle, K., Wallace, L., Valenti, J., & Harmer, D. 2000, *Visible and Near Infrared Atlas of the Arcturus Spectrum 3727-9300 A* 3
- Hozumi, S., & Burkert, A. 2015, *MNRAS*, 446, 3100 1
- Kundu, R., Minniti, D., & Singh, H. P. 2019, *MNRAS*, 483, 1737 2, 3, 6, 7, 8
- Kurucz, R. L. 1970, *SAO Special Report*, 309 5
- Kurucz, R. L. 2005, *Memorie della Societa Astronomica Italiana Supplementi*, 8, 14 5
- Mackey, A. D., Ferguson, A. M. N., Huxor, A. P., et al. 2019, *MNRAS*, 484, 1756 1
- Malhan, K., Valluri, M., & Freese, K. 2021, *MNRAS*, 501, 179 1, 6
- Malhan, K., Valluri, M., Freese, K., & Ibata, R. A. 2022, *ApJ*, 941, L38 6
- Marino, A. F., Milone, A. P., Renzini, A., et al. 2019, *MNRAS*, 487, 3815 7
- Massari, D., Mucciarelli, A., Dalessandro, E., et al. 2017, *MNRAS*, 468, 1249 4, 6, 7, 8
- Mestre, M., Llinares, C., & Carpintero, D. D. 2020, *MNRAS*, 492, 4398 2
- Moreno, E., Pichardo, B., & Velázquez, H. 2014, *ApJ*, 793, 110 2
- Mucciarelli, A., Dalessandro, E., Massari, D., et al. 2016, *ApJ*, 824, 73 3, 5
- Nissen, P. E., & Schuster, W. J. 2010, *A&A*, 511, L10 6, 7
- Osterbrock, D. E., Fulbright, J. P., Martel, A. R., et al. 1996, *PASP*, 108, 277 3
- Pancino, E., Marrese, P. M., Marinoni, S., et al. 2022, *A&A*, 664, A109 4
- Pasquini, L., Avila, G., Blecha, A., et al. 2002, *The Messenger*, 110, 1 2
- Piatti, A. E. 2017, *ApJ*, 834, L14 3
- Piatti, A. E. 2023, *MNRAS*, 525, L72 2, 7
- Piatti, A. E. 2024, *A&A*, 683, A151 4, 6, 7
- Piatti, A. E., Illesca, D. M. F., Massara, A. A., et al. 2023, *MNRAS*, 518, 6216 6
- Reddy, B. E., Lambert, D. L., & Allende Prieto, C. 2006, *VizieR Online Data Catalog: Elemental abundances for 176 stars (Reddy+, 2006)*, *VizieR On-line Data Catalog: J/MNRAS/367/1329*. Originally published in: 2006MNRAS.367.1329R 7
- Reddy, B. E., Tomkin, J., Lambert, D. L., & Allende Prieto, C. 2003, *MNRAS*, 340, 304 7
- Snedden, C. A. 1973, *Carbon and Nitrogen Abundances in Metal-Poor Stars.*, PhD thesis, University of Texas, Austin 4
- Sobeck, J. S., Kraft, R. P., Sneden, C., et al. 2011, *AJ*, 141, 175 4
- Sollima, A. 2020, *MNRAS*, 495, 2222 2, 6
- Stetson, P. B., & Pancino, E. 2008, *PASP*, 120, 1332 4
- Tonry, J., & Davis, M. 1979, *AJ*, 84, 1511 3

- Vasiliev, E. 2019, MNRAS, 484, 2832 2
- Venn, K. A., Irwin, M., Shetrone, M. D., et al. 2004, AJ, 128, 1177 7
- Venn, K. A., Starkenburg, E., Malo, L., Martin, N., & Laevens, B. P. M. 2017, MNRAS, 466, 3741 4
- Wan, Z., Oliver, W. H., Baumgardt, H., et al. 2021, MNRAS, 502, 4513 2
- Xu, C., Tang, B., Li, C., et al. 2024, A&A, 684, A205 6
- Zhang, S., Mackey, D., & Da Costa, G. S. 2022, MNRAS, 513, 3136 1